ADVANCES IN ATMOSPHERIC SCIENCES, VOL. 40, FEBRUARY 2023, 194–200

• News & Views •

Ground–Space–Sky Observing System Experiment during Tropical Cyclone Mulan in August 2022

Pak-wai CHAN[1], Wei HAN[2], Betty MAK[1], Xiaohao QIN[*3], Yongzhu LIU[2], Ruoying YIN[2], and Jincheng WANG[2]

[1]*Hong Kong Observatory*, *Hong Kong*, *China*

[2]*China Meteorological Administration Earth System Modeling and Prediction Centre*, *Beijing* 100081, *China*

[3]*State Key Laboratory of Numerical Modeling for Atmospheric Sciences and Geophysical Fluid Dynamics*, *Institute of Atmospheric Physics*, *Chinese Academy of Sciences*, *Beijing* 100029, *China*

(Received 19 September 2022; revised 30 September 2022; accepted 9 October 2022)

ABSTRACT

Forecasting tropical cyclone track and intensity is a great challenge for the meteorological community, and safeguarding the life and property of people living near the coast is an important issue. One major reason for challenging forecasts is the lack of observations over the vast oceans. During tropical cyclone Mulan between 8 and 10 August 2022 over the northern part of the South China Sea, the meteorological authority and research institutes of Chinese mainland collaborated with the meteorological service in Hong Kong on conducting the first-ever ground–space–sky observing system experiment on tropical cyclone Mulan. The enhanced targeted observations collected during the experiment include Geostationary Interferometric Infrared Sounder, round-trip radiosondes, and aircraft-launched dropsondes. This paper describes the campaign, technical details of the meteorological models used, and impact of the additional targeted observation data on the tropical cyclone forecast. Ideally, similar enhanced observation campaigns could be conducted in the future, not only in the northern part of the South China Sea, but also in other ocean basins.

Key words: ground–space–sky, observing system experiment, TC Mulan (2022)

Citation: Chan, P.-W., W. Han, B. Mak, X. H. Qin, Y. Z. Liu, R. Y. Yin, and J. C. Wang, 2023: Ground–space–sky observing system experiment during tropical cyclone Mulan in August 2022. *Adv. Atmos. Sci.*, **40**(2), 194–200, https://doi.org/10.1007/s00376-022-2267-z.

1. Introduction

In summer, tropical cyclones (TCs) develop over the Northwestern Pacific or the South China Sea (SCS), and some move towards the coasts of southern and eastern China. They may cause severe property damage and loss of life. Monitoring and forecasting TCs are great challenges for meteorological services institutes because of the limited number of meteorological observations over the vast oceans. With the use of meteorological satellites, it is possible to monitor the movement and development of convective clouds associated with TCs and thus to track TCs and estimate their intensities. However, upper-air measurements of wind, temperature, humidity, and pressure inside and around TCs are lacking, which limits the analysis of the circulation and intensity of TCs as well as their forecasting using numerical weather prediction (NWP) models.

In recent years, more in situ and remote sensing observations of TCs have become available over the SCS. This includes dropsonde observations from a fixed-wing aircraft operated by the Government Flying Service (GFS) of the Hong Kong Government when TCs enter the flight information region (FIR) of Hong Kong. The Geostationary Interferometric Infrared Sounder (GIIRS) on board the FengYun-4B satellite (FY-4B) of the China Meteorology Administration (CMA) remotely measures temperature and dew point profiles of the atmosphere from the space. Ground-based measurements include retractable meteorological balloons over South China. Such measurements help fill up the meteorological data void

* Corresponding author: Xiaohao QIN
Email: xhqin@lasg.iap.ac.cn

over the northern part of the SCS as well as surrounding areas for enhanced monitoring of TCs and their environmental meteorological conditions.

The above new observation platforms are normally operated separately. But in the period from 8 to 10 August 2022, collaborative observing system experiments (OSEs) were simultaneously conducted to capture the three-dimensional structure of TC Mulan (2022) over the northern part of the SCS. This is the first collaborative effort between the CMA, Institute of Atmospheric Physics (IAP) of Chinese Academy of Sciences, Fudan University, and the Hong Kong Observatory (HKO) to work together for real-time, three-dimensional monitoring of a TC from a ground–space–sky platform. To determine the scanning area of the FY-4B, which enables a module with finer spatial–temporal resolutions, and to plan the dropsonde launches, the singular vectors approach (SVs; Palmer et al., 1998) was used to identify a primary area, and then the IAP-developed conditional nonlinear optimal perturbation method (CNOP; Mu et al., 2003, 2009; Qin et al., 2022) was further applied to refine this area and finally provide the sensitive area for targeted observations for the FY-4B and dropsondes launches three days ahead of the real-time conduction (i.e., approximately at 0600 UTC on 5 August for that planned on 8 August, etc.). Moreover, the meteorological data were ingested in real time into the self-developed NWP modeling system of the CMA. The observational and forecast results were presented in the morning weather conferences of the CMA. This campaign of OSEs is the first of its kind conducted in China.

This paper documents the meteorological equipment and NWP-related software used in the OSEs. The meteorological observations and the preliminary verifications of the forecast results are presented. More similar campaigns may be conducted in the future over the SCS to better quantify the impacts of advanced meteorological measurements on TC forecasts.

2. Meteorological equipment

2.1. *Dropsonde*

The HKO has been collaborating with the GFS on dropsonde TC reconnaissance flights since 2016 (Chan et al., 2018). The HKO uses data from the Airborne Vertical Atmospheric Profiling System (AVAPS) commercialized by Vaisala and installed on the GFS fixed-wing aircraft and manual RD41 dropsonde units.

With the approach of a TC, one of the two fixed-wing aircraft would be engaged for dropsonde operation at the request of the HKO. A dropsonde release plan is drawn based on the predicted TC location at the time of mission, balancing the needs for TC monitoring by the forecasting office and TC forecasting by numerical models. Flight plans are normally submitted 48–72 hours in advance. Currently the operating area covers the Hong Kong FIR and is 250 km away from the Hong Kong International Airport. Readers may refer to the later section on the operation for TC Mulan (2022) and figures therein for more detail.

The launched dropsonde descends to the sea surface with the help of a parachute. Pressure, temperature, and humidity data are measured twice per second, and wind is measured four times per second. The data is transmitted via radio band telemetry link to the receiving AVAPS on board the aircraft. The received data is then relayed via the onboard SAT-COM equipment to the HKO's ground station server in real time. The received data goes through a quality control [QC; details can be found in Rousseeuw (1987), Paraskevopoulou et al. (2013), and Lu and Zhou, (2016)] process before being provided to the forecasting team for TC operations; it is also converted to BUFR format for global dissemination through the Global Telecommunication System.

2.2. *GIIRS on board FY-4B*

The GIIRS is a hyperspectral infrared (IR) sounder on board a geostationary weather satellite. The FY-4B carrying GIIRS was launched on 3 June 2021, and similar to the GIIRS on FY-4A, it provides unprecedented continuous temperature and humidity profiles with high temporal, spatial, and vertical resolutions, which is valuable for monitoring, warning, and forecasting high-impact weather events (Schmit et al., 2009; Li et al., 2011; Yin et al., 2021). The FY-4B GIIRS has 1682 spectral channels, including 721 longwave (LW) IR channels (680–1130 cm^{-1}) and 961 middlewave IR channels (1650–2250 cm^{-1}). It has the capability of scanning the atmosphere quickly [e.g., 15 minutes for TC Mulan (2022) in this study] at a spectral interval of 0.625 cm^{-1} and a spatial horizontal resolution of about 12 km.

2.3. *Round-trip drift radiosonde*

The CMA has developed a new type of round-trip drift radiosonde observation technology (Cao et al., 2019). Compared to conventional radiosonde techniques, this technology enables two vertical troposphere–stratosphere soundings (ascending and descending) and four-hour continuous observations of the stratosphere at specified height (>20 km) without significantly increased costs. A typical observation process lasts for six hours or longer, and the data precision has reached the criterion defined by the World Meteorological Organization (Guo et al., 2020; Wang et al., 2020).

3. NWP-related software

3.1. *SVs and CNOP*

SVs are defined as a group of mutually orthogonal initial perturbations that maximize the growth rate over a finite time in terms of a norm, which is fulfilled by the tangent linear model of an NWP. The SVs in the Global and Regional Assimilation and PrEdiction System (GRAPES) model are calculated by solving the eigenvalue problem in the Eq. (1) based on the Lanczos algorithm (Simon, 1984):

$$\left(E^{-\frac{1}{2}}L^{\mathrm{T}}P^{\mathrm{T}}EPLE^{-\frac{1}{2}}\right)\widehat{\boldsymbol{X}}_i(t_0)=\lambda_i^2\widehat{\boldsymbol{X}}_i(t_0)\ , \tag{1}$$

where $\widehat{\boldsymbol{X}}_i(t_0)$ is the transformation of the Euclidean vector of the initial perturbations $\boldsymbol{X}_i(t_0)$, L^{T} is the adjoint model of tangent linear model L of an NWP, and λ measures the growth rate of initial perturbation at the final time in terms of a norm E. It should be noted that the SVs were computed by confining the perturbation vectors to occur in the regions of (30°–80°N, 80°–30°S) through the project P; and the area identified by SVs in this study was a composite of the vertically integrated total perturbation energy (E; Palmer et al., 1998; Liu et al., 2013) of the leading fifteen SVs, weighted by the ratio of the corresponding singular value to that of the leading one.

The CNOP represents the initial perturbation that satisfies a certain physical constraint and leads to the largest forecast error at the final time induced by nonlinear evolution (Mu et al., 2003). The CNOP is a natural generalization of the leading SV in nonlinear regime and fully considers the effect of nonlinear physical processes. For TC forecasting, it has been shown that the CNOP is superior to the SVs in identifying the sensitive area for targeted observations (Mu et al., 2009; Qin and Mu, 2012; Qin et al., 2022). In addition, the CNOP has also been used to identify the sensitive areas for targeted observations associated with the forecasting of other high-impact climate and weather events such as El Niño-Southern Oscillation, the Indian Ocean Dipole, heavy air pollution events, southwest vortices, oceanic mesoscale eddies, and the vertical thermal structure in the Yellow Sea (Mu et al., 2017; Duan et al., 2018; Chen et al., 2021; Hu et al., 2021; Jiang et al., 2022; Yang et al., 2022).

Based on the area identified by the SVs, the CNOP method was applied to refine and identify the sensitive area on 5 August using the Weather Research and Forecasting model and its adjoint model, with the aim being to determine the best scanning area of the FY-4B and best dropsonde launch locations for the period 8–10 August in order to improve both the track and intensity forecasts for TC Mulan (2022) in the following three days. Furthermore, we kept recalculating and updating the sensitive areas using the latest forecasts issued by the ECMWF during the period 6–8 August, in order to ensure the accuracy of the identified sensitive regions as TC Mulan (2022) developed. The updated results showed that the sensitive areas for collaborative measurements planned on 9 and 10 August were located around Leizhou Peninsula and were further westward than those identified earlier, which suggested a probability of westward movement of TC Mulan (2022) in the subsequent days.

3.2. *GRAPES data assimilation system*

The GRAPES global four-dimensional variational (4D-Var) data assimilation system was developed by the numerical weather prediction center of the CMA in 2008 and has been operated since July 2018 (Zhang et al., 2019). The details of the dynamical framework of the GRAPES atmospheric model can be found in Chen et al. (2012). Note that a series of linear physical processes and the incremental analysis scheme (Courtier et al., 1994) are applied to the GRAPES 4D-Var assimilation system, which aims to solve the minimization problem of the cost function in the Eq. (2) (Liu et al., 2018).

$$J(\delta\boldsymbol{x})=\frac{1}{2}\left(\delta\boldsymbol{x}-\left(\boldsymbol{x}_{\mathrm{b}}-\boldsymbol{x}_{\mathrm{g}}\right)\right)^{\mathrm{T}}\boldsymbol{B}^{-1}\left(\delta\boldsymbol{x}-\left(\boldsymbol{x}_{\mathrm{b}}-\boldsymbol{x}_{\mathrm{g}}\right)\right)+\frac{1}{2}\sum_{i=0}^{n}(H_iM_{0\to i}\delta\boldsymbol{x}+\boldsymbol{d}_i)^{\mathrm{T}}\boldsymbol{R}_i^{-1}(H_iM_{0\to i}\delta\boldsymbol{x}+\boldsymbol{d}_i)+J_{\mathrm{c}}, \tag{2}$$

where $\boldsymbol{x}_{\mathrm{b}}$ is the background state; $\boldsymbol{x}_{\mathrm{g}}$ is the first guess; $\delta\boldsymbol{x}=\boldsymbol{x}-\boldsymbol{x}_{\mathrm{g}}$ is the analysis increment of the model variables; $\boldsymbol{d}_i=H_iM_{0\to i}\left(\boldsymbol{x}_{\mathrm{g}}\right)-\boldsymbol{y}_i$ is the observation increment at time i; H_i is the observation operator at time i; $M_{0\to i}$ is the model integration from the analysis time to time i; $\boldsymbol{y}_i$ is the observation at time i; $\boldsymbol{B}$ is the error covariance matrix of $\boldsymbol{x}_{\mathrm{b}}$; $\boldsymbol{R}_i$ is the observational error covariance matrix at time i; and J_{c} is the weak constraint term based on the digital filter. To reduce the computational cost of the minimization, $\delta\boldsymbol{x}$ and $\boldsymbol{B}$ are defined on a lower resolution grid than $\boldsymbol{x}_{\mathrm{b}}$ and $\boldsymbol{x}_{\mathrm{g}}$. The interpolation operator is introduced to act on $\boldsymbol{x}_{\mathrm{b}}$ and$\boldsymbol{x}_{\mathrm{g}}$.

4. Observations

4.1. *Dropsonde observations*

As seen from the wind measurements (Fig. 1) obtained over the northern part of the SCS during the campaign, TC

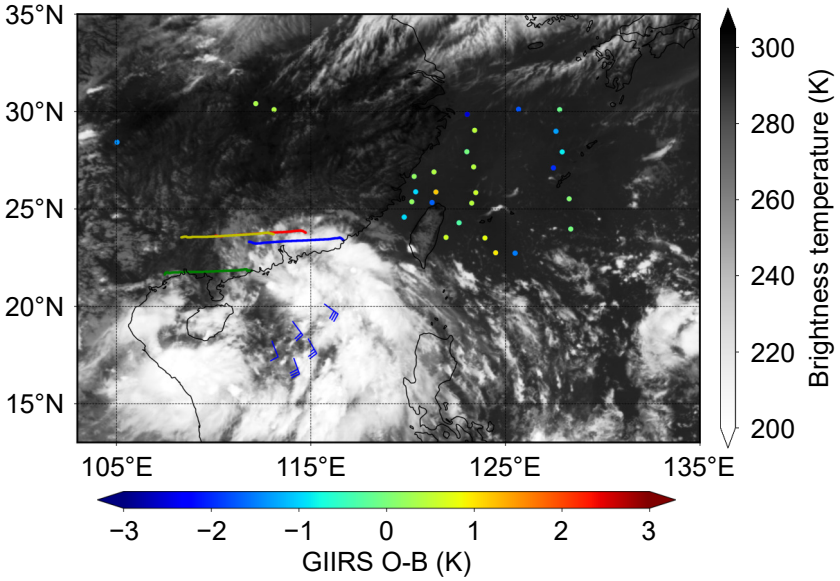

Fig. 1. Overview of the ground–space–sky observations on 9 August: brightness temperature from AGRI (K), wind vectors from dropsondes (blue wind barbs; knots), and round-trip drift radiosonde (colored lines). Colored dots denote the differences between observations and simulations after quality control of the GIIRS longwave channel 32 (699.375 cm^{-1}) at 0530 UTC 9 August.

Mulan (2022) showed the properties of a monsoon depression, i.e., the winds around the center of TC Mulan (2022) were relatively weak, while the winds in the outer rainband to the west of the Philippines were much stronger. Such strong winds could affect the Pearl River Estuary area of South China.

4.2. *GIIRS observations*

A 3D targeted observing operation was performed for TC Mulan (2022) using FY-4B GIIRS starting at 0000 UTC on 8 August 2022. During this period, GIIRS observed a fixed area (10°–35°N, 110°–130°E) affected by TC Mulan (2022) at a temporal resolution of 15 minutes (see Fig. 1). Thirty-eight LW channels were selected for assimilation in this case by using the entropy iteration method (Yin et al., 2019). These channels cover the upper, middle, and lower troposphere and provide critical information on atmospheric vertical structures for data assimilation and model forecasts. In this study, the thinning mesh for GIIRS radiances is every 100 km. The cloud detection, bias correction, and other QC schemes for GIIRS can be found in Yin et al. (2020). The differences between observations and simulations after QC of the LW channel 32 (699.375 cm^{-1}) at 0530 UTC on 9 August are indicated as colored dots in Fig. 1.

4.3. *Round-trip drift radiosonde observations*

From the end of July 2022, the round-trip drift radiosonde observation experiment is being carried out at four sounding stations in Guangdong. The horizontal trajectories of round-trip drift radiosondes released at 0530 UTC on 9 August are shown as the colored lines in Fig. 1.

5. Numerical experiments

5.1. *Analysis field*

The analysis field of GRAPES appears to be improved with the ingestion of the additional targeted observation data. For instance, the analysis of the geopotential at 500 hPa at 0600 UTC on 8 August (Fig. 2a) shows two low pressure centers over the SCS, compared with only one center in the forecast without the additional observations. The two-center analysis appears to be more consistent with the two connected cloud systems observed by the satellite in this region (Fig. 2b). The additional observation data helps to better resolve the two-center feature of the relatively weak low pressure system over the SCS.

5.2. *Observations minus background*

The meteorological observations from retractable balloons and dropsondes minus the background field of the NWP model (OMB) are inspected (not shown). The OMBs are rather significant. The OMBs for the U and V components of the

wind reach about 5 m s^{-1}. Those for temperatures and relative humidity reach about 2 K and as large as 50%, respectively. As such, the additional meteorological observations could have significant impacts on the GRAPES forecast.

5.3. *TC track and intensity forecasts*

The forecast tracks before and after the ingestion of the additional targeted observation data are shown in Fig. 3a. Without these data, the TC track forecast initiated at 0600 UTC on 8 August was relatively smooth, and the TC was forecasted to move generally in a northwestward direction. After assimilating the additional data, the TC was forecasted to move westward firstly and then northward, which is closer to the observation.

The TC intensity forecasts without and with the additional meteorological data are shown in Fig. 3b. With the additional targeted observation data, the forecast intensity of this relatively weak system showed smaller errors, with a reduction of about 11%. This improvement persisted up to the 36-h forecast.

5.4. *Rainfall forecasts*

The rainfall distribution forecasts and the Equitable Threat Score (ETS) for the model runs initiated at 0000 UTC 10 August are shown in Fig. 4. The 24-hour accumulated rainfall is considered. It can be seen that, compared with the forecast without additional targeted observations, the one with them was able to provide better results for higher rainfall categories; for rainfall category at or greater than 25 mm, there is a reduction of false alarms by three stations (eight stations to five stations); for rainfall category at or greater than 50 mm, two more stations are accurately forecast (five stations increasing to seven stations), and missed forecasts are reduced by two stations (twenty-seven stations reducing to twenty-five stations).

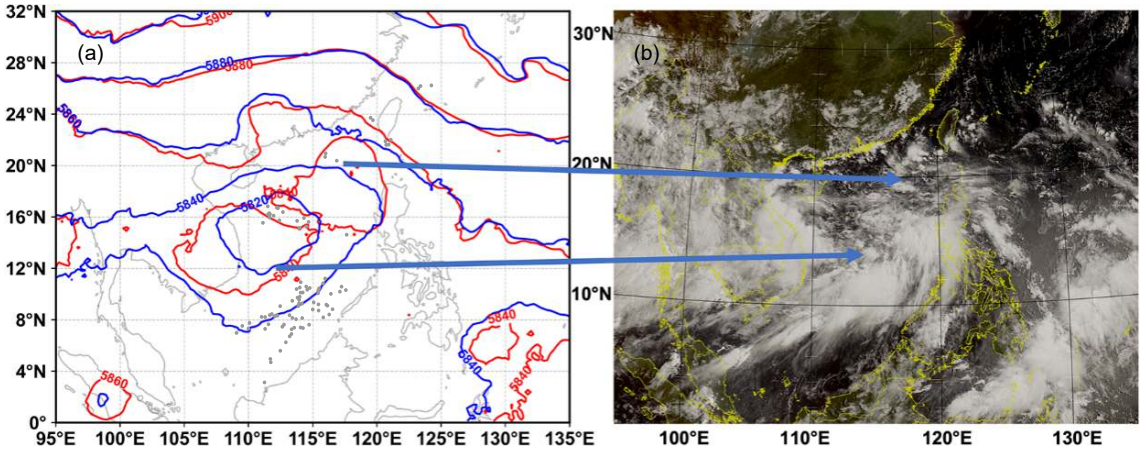

Fig. 2. (a) The analysis field of the geopotential (gpm) at 500 hPa at 0600 UTC on 8 August 2022 before (blue) and after (red) ingestion of additional observations. The corresponding satellite image is shown in (b).

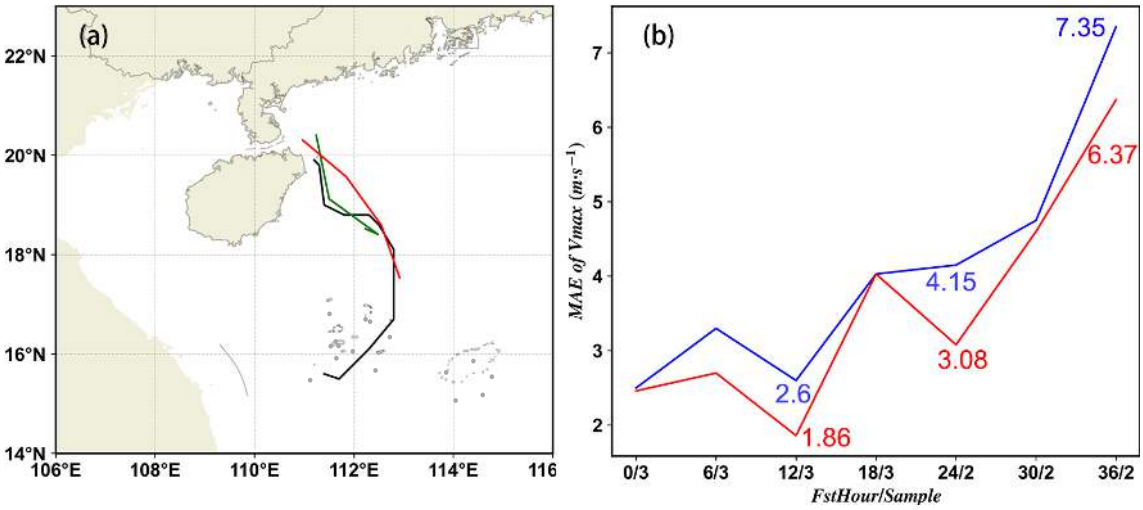

Fig. 3. (a) Forecast tracks of TC Mulan (2022) before (red) and after (green) assimilating additional observations. The black line denotes the best track. (b) Forecast errors (m s^{-1}) of the V_{max} before (blue) and after (red) assimilating additional observations.

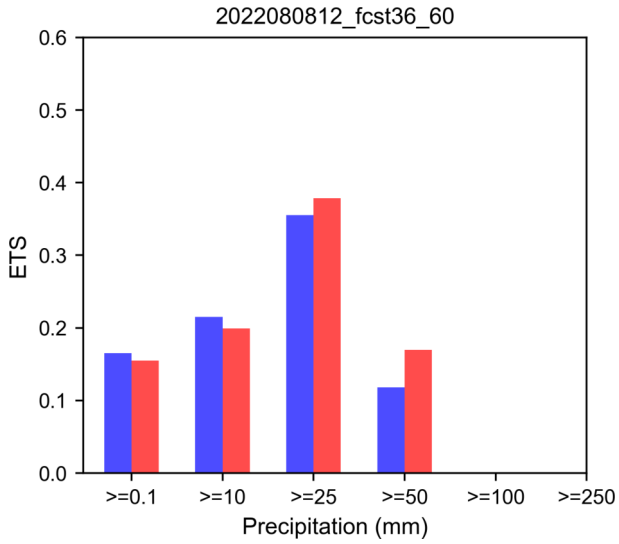

Fig. 4. The ETS before (blue) and after (red) assimilating additional targeted observations for different rainfall categories (mm).

As such, the ETSs for the 25 mm and 50 mm categories are higher. On the other hand, the ETSs for the 0.1 mm and 10 mm categories remain basically similar.

6. Conclusion

The first ground–space–sky collaborative OSEs for TC Mulan in August 2022 are documented in this paper. This campaign is state-of-the-art and provided valuable targeted observation data for testing how TC forecasts can be improved with the use of modern in situ and remote sensing data. The campaign was conducted smoothly, and the data obtained were ingested in real time into the NWP system and used in morning weather conferences. The use of the CNOP and the GRAPES 4D-Var represents the real-time implementation of self-developed technologies in China to support meteorological observational campaigns and weather forecasters. The additional data collected resulted in positive impacts on forecasts of TC movement, intensity, and heavy rain impacts on southern China.

With the success of the present campaign, more experiments will be conducted in the future for TCs over the northern part of the SCS in order to more systematically assess the performance and usefulness of the new data. The results will be presented in future papers.

Acknowledgements. This study was adjointly supported by the National Natural Science Foundation of China (Grant Nos. 41930971 and 42075155).

REFERENCES

Cao, X. Z., Q. Y. Guo, and R. K. Yang, 2019: Research of rising and falling twice sounding based on long-time interval of flat-floating. *Chinese Journal of Scientific Instrument*, **40**(2), 198–204, https://doi.org/10.19650/j.cnki.cjsi.J1803748. (in Chinese with English abstract)

Chan, P. W., N. G. Wu, C. Z. Zhang, W. J. Deng, and K. K. Hon, 2018: The first complete dropsonde observation of a tropical cyclone over the South China Sea by the Hong Kong Observatory. *Weather*, **73**, 227–234, https://doi.org/10.1002/wea.3095.

Chen, D. H., J. S. Xue, X. S. Shen,, J. Sun, Q. L. Wan, Z. Y. Jin, and X. L. Li, 2012: Application and prospect of a new generation of numerical weather prediction system (GRAPES). *Strategic Study of CAE.*, **14**(9), 46–54.

Chen, G., B. Wang, and J. J. Liu, 2021: Study on the sensitivity of initial perturbations to the development of a vortex observed in Southwest China. *J. Geophys. Res.: Atmos.*, **126**, e2021JD034715, https://doi.org/10.1029/2021JD034715.

Courtier, P., J. N. Thépaut, and A. Hollingsworth, 1994: A strategy for operational implementation of 4D-Var, using an incremental approach. *Quart. J. Roy. Meteor. Soc.*, **120**(519), 1367–1387, https://doi.org/10.1002/qj.49712051912.

Duan, W. S., X. Q. Li, and B. Tian, 2018: Towards optimal observational array for dealing with challenges of El Niño-Southern Oscillation predictions due to diversities of El Niño. *Climate Dyn.*, **51**, 3351–3368, https://doi.org/10.1007/s00382-018-4082-x.

Guo, Q. Y., R. K. Yang, K. Q. Cheng, and C. X. Li, 2020: Refractive index quality control and comparative analysis of multi-source occultation based on sounding observation. *Journal of Applied Meteorological Science*, **31**(1), 13–26, https://doi.org/10.11898/1001-7313.20200102. (in Chinese with English abstract)

Hu, H. Q., J. Y. Liu, L. L. Da, W. H. Guo, K. Liu, and B. L. Cui, 2021: Identification of the sensitive area for targeted observation to improve vertical thermal structure prediction in summer in the Yellow Sea. *Acta Oceanologica Sinica*, **40**(7), 77−87, https://doi.org/10.1007/s13131-021-1738-x.

Jiang, L., W. S. Duan, and H. L. Liu, 2022: The most sensitive initial error of sea surface height anomaly forecasts and its implication for target observations of mesoscale eddies. *J. Phys. Oceanogr.*, **52**, 723−740, https://doi.org/10.1175/JPO-D-21-0200.1.

Li, J., J. L. Li, J. Otkin, T. J. Schmit, and C. Y. Liu, 2011: Warning information in a preconvection environment from the geostationary advanced infrared sounding system - A simulation study using the IHOP case. *J. Appl. Meteorol. Climatol.*, **50**, 776−783, https://doi.org/10.1175/2010JAMC2441.1.

Liu, Y. Z., X. S. Shen, and X. L. Li, 2013: Research on the singular vector perturbation of the GRAPES global model based on the total energy norm. *Acta Meteorologica Sinica*, **71**(3), 517−526, https://doi.org/10.11676/qxxb2013.043. (in Chinese with English abstract)

Liu, Y. Z., L. Zhang, and Z. H. Lian, 2018: Conjugate gradient algorithm in the four-dimensional variational data assimilation system in GRAPES. *Journal of Meteorological Research*, **32**(6), 974−984, https://doi.org/10.1007/s13351-018-8053-2.

Lu, Y., and H. H. Zhou, 2016: Statistical and computational guarantees of Lloyd's algorithm and its variants. arXiv: 1612.02099, https://doi.org/10.48550/arXiv.1612.02099.

Mu, M., W. S. Duan, and B. Wang, 2003: Conditional nonlinear optimal perturbation and its applications. *Nonlinear Processes in Geophysics*, **10**, 493−501, https://doi.org/10.5194/npg-10-493-2003.

Mu, M., F. F. Zhou, and H. L. Wang, 2009: A method for identifying the sensitive areas in targeted observations for tropical cyclone prediction: Conditional nonlinear optimal perturbation. *Mon. Wea. Rev.*, **137**, 1623−1639, https://doi.org/10.1175/2008MWR2640.1.

Mu, M., R. Feng, and W. S. Duan, 2017: Relationship between optimal precursors for Indian Ocean Dipole events and optimally growing initial errors in its prediction. *J. Geophys. Res.: Oceans*, **122**, 1141−1153, https://doi.org/10.1002/2016JC012527.

Palmer, T. N., R. Gelaro, J. Barkmeijer, and R. Buizza, 1998: Singular vectors, metrics, and adaptive observations. *Journal of the Atmospheric Sciences*, **55**, 633−653, https://doi.org/10.1175/1520-0469(1998)055<0633:SVMAAO>2.0.CO;2.

Paraskevopoulou, S. E., D. Y. Barsakcioglu, M. R. Saberi, A. Eftekhar, and T. G. Constandinou, 2013: Feature extraction using first and second derivative extrema (FSDE) for real-time and hardware-efficient spike sorting. *Journal of Neuroscience Methods*, **215**(1), 29−37, https://doi.org/10.1016/j.jneumeth.2013.01.012.

Qin, X. H., and M. Mu, 2012: Influence of conditional nonlinear optimal perturbations sensitivity on typhoon track forecasts. *Quart. J. Roy. Meteor. Soc.*, **138**, 185−197, https://doi.org/10.1002/qj.902.

Qin, X. H., W. S. Duan, P.-W. Chan, B. Y. Chen, and K.-N. Huang, 2022: Effects of dropsonde data in field campaigns on forecasts of tropical cyclones over the western North Pacific in 2020 and the role of CNOP sensitivity. *Adv. Atmos. Sci.*, https://doi.org/10.1007/s00376-022-2136-9.

Rousseeuw, P. J., 1987: Silhouettes: A graphical aid to the interpretation and validation of cluster analysis. *Journal of Computational and Applied Mathematics*, **20**, 53−65, https://doi.org/10.1016/0377-0427(87)90125-7.

Schmit, T. J., J. Li, S. A. Ackerman, and J. J. Gurka, 2009: High-spectral- and high-temporal-resolution infrared measurements from geostationary orbit. *J. Atmos. Oceanic Technol.*, **26**(11), 2273−2292, https://doi.org/10.1175/2009jtecha1248.1.

Simon, H. D., 1984: The Lanczos algorithm with partial reorthogonalization. *Mathematics of Computation*, **42**(165), 115−142, https://doi.org/10.2307/2007563.

Wang, D., J. C. Wang, W. H. Tian, and Q. Y. Guo, 2020: Quality control and uncertainty analysis of return radiosonde data. *Chinese Journal of Atmospheric Sciences*, **44**(4), 865−884, https://doi.org/10.3878/j.issn.1006-9895.1912.19203. (in Chinese with English abstract)

Yang, L. C., W. S. Duan, Z. F. Wang, and W. Y. Yang, 2022: Toward targeted observations of the meteorological initial state for improving the $PM_{2.5}$ forecast of a heavy haze event that occurred in the Beijing-Tianjin-Hebei region. *Atmospheric Chemistry and Physics*, 22, 11 429−11 453, https://doi.org/10.5194/ACP-22-11429-2022.

Yin, R. Y., W. Han, Z. Q. Gao, and G. Wang, 2019: A study on longwave infrared channel selection based on estimates of background errors and observation errors in the detection area of FY-4A. *Acta Meteorologica Sinica*, **77**(5), 898−910, https://doi.org/10.11676/qxxb2019.051. (in Chinese with English abstract)

Yin, R. Y., W. Han, Z. Q. Gao, and D. Di, 2020: The evaluation of FY4A's Geostationary Interferometric Infrared Sounder (GIIRS) long-wave temperature sounding channels using the GRAPES global 4D-Var. *Quart. J. Roy. Meteor. Soc.*, **146**, 1459−1476, https://doi.org/10.1002/qj.3746.

Yin, R. Y., W. Han, Z. Q. Gao, and J. Li, 2021: Impact of high temporal resolution FY-4A Geostationary Interferometric Infrared Sounder (GIIRS) radiance measurements on Typhoon forecasts: Maria (2018) case with GRAPES global 4D-Var assimilation system. *Geophys. Res. Lett.*, **48**, e2021GL093672, https://doi.org/10.1029/2021GL093672.

Zhang, L., and Coauthors, 2019: The operational global four-dimensional variational data assimilation system at the China Meteorological Administration. *Quart. J. Roy. Meteor. Soc.*, **145**, 1882−1896, https://doi.org/10.1002/qj.3533.